Decadal evolution of carbon sink within a strong bloom area in the subantarctic zone

Anna Lourantou, Nicolas Metzl

Decadal evolution of carbon sink within a strong bloom area in the subantarctic zone

Anna Lourantou[1] and Nicolas Metzl[1]

Received 14 September 2011; revised 2 November 2011; accepted 5 November 2011; published 13 December 2011.

[1] The fate of the Southern Ocean atmospheric CO_2 sink is under question. Here we assess seasonal to decadal changes of surface fCO_2 within an extended sink area along the track between Kerguelen and Amsterdam islands in the subantarctic zone. Data from 17 oceanographic cruises were used, from 1991 to 2011 and two distinct regions were examined, separated by the Subantarctic Front (SAF). The region south of the SAF displays a strong summer phytoplankton bloom of up to -28 mmol C m^{-2} d^{-1} within a calm area, constrained by physics and topography. On an annual basis, this region is a 6-fold more important sink than that deduced from Takahashi climatology, highlighting the importance of key-areas separate examination before proceeding to spatial integration. Our data point towards a decadal decline of the CO_2 sink in the Southern part of the SAF, most probably due to both warming and less Fe input to surface waters from reduced water mixing.

Citation: Lourantou, A., and N. Metzl (2011), Decadal evolution of carbon sink within a strong bloom area in the subantarctic zone, *Geophys. Res. Lett.*, *38*, L23608, doi:10.1029/2011GL049614.

1. Introduction

[2] The Southern ocean is considered a major player in the climate system at different time scales, from glacial-interglacial transitions [*Lourantou et al.*, 2010a, 2010b] up to modern time where it removes about 10% of the global CO_2 emissions [*Takahashi et al.*, 2009]. The Subantarctic Zone (SAZ, [35–50]°S), a key area for mode waters formation and anthropogenic carbon isolation [*Metzl et al.*, 1999; *Sabine et al.*, 2004; *Mikaloff Fletcher et al.*, 2006], constitutes one of the most efficient atmospheric CO_2 sinks [*Takahashi et al.*, 2009]. This important sink is linked with extended phytoplankton blooms occurring every austral summer downstream of subantarctic islands, which contrasts the High Nutrient Low Chlorophyll (HNLC) character of Southern Ocean waters.

[3] CROZEX and KEOPS summer cruises in 2004 and 2005 examined the role of Crozet and SE Kerguelen plateaus (French Southern Territories), respectively, highlighting the "island mass effect" theory [*Doty and Oguri*, 1956]. These studies revealed that waters downstream of these islands are fuelled with Fe (the limiting micronutrient for HNLC areas [*Martin*, 1991]) from the seafloor [*Planquette et al.*, 2007; *Blain et al.*, 2007, 2008; *Chever et al.*, 2010]. This enhances marine productivity, as depicted in satellite-derived chlorophyll-a (chla) images [*Mongin et al.*, 2008] and results in surface fCO_2 (f for fugacity) drawdown [*Bakker et al.*, 2007; *Jouandet et al.*, 2008]. The NE Kerguelen plateau, situated within the SAZ, north of the Polar Front (separating it from the SE Kerguelen plateau [*Park et al.*, 2008]) and south of a complex system merging Subtropical and Subantarctic fronts [*Park et al.*, 1993], also experiences a significant summer bloom. This area has been examined once in 1995 during ANTARES3/JGOFS cruise [*Blain et al.*, 2001], albeit with no surface fCO_2 information provided.

[4] All above case studies supply vital data, although restricted in space and time. A seasonal to decadal air-sea CO_2 fluxes (FCO_2) monitoring within such intense bloom areas, is missing. This would provide further constraints on modeling [*Le Quéré et al.*, 2007] or observational studies over more extended areas [*Metzl*, 2009] that speculate a decreasing Southern ocean sink pattern. This study investigates the fCO_2 dynamics along the track between Kerguelen (49°15′S; 69°35′E) and Amsterdam (37°49′S; 77°33′E) islands, out of 17 cruises implemented from 1991 to 2011. The NE Kerguelen plateau is located at the southern extreme of this track, at the southern part of the SAF (SSAF). The summer bloom is first separately studied by combining biological, physical and bathymetric elements (section 3.1). Seasonal hydrological and fCO_2 changes are then assessed, together with integrated annual FCO_2 computing (section 3.2) for both the SSAF and the northern part of the SAF (NSAF). This study ends with evaluations on the driving mechanisms and the decadal trends in both regions across the SAF (section 3.3).

2. Cruises Presentation, Data Resources, FCO_2 Computing

[5] The tracks and periods for all studied cruises are shown in Figure 1. These campaigns were conducted in the framework of MINERVE (Mesures à l'INterface Eau-aiR, Variabilité des Echanges de CO_2, thereinafter referred to as "min") and OISO (Océan Indien Service d'Observation) programs, onboard the *R/V Marion Dufresne I&II*. A similar analytical protocol is applied for sea surface data acquisition for all cruises (cf. auxiliary material).[1] The majority of the fCO_2 data presented here, together with bathymetric and atmospheric CO_2 data, has been provided from the Surface Ocean CO_2 Atlas (SOCAT), a new international database joining surface fCO_2 measurements issued from cruises since 1968 (http://www.socat.info (B. Pfeil et al., A uniform, quality controlled, Surface Ocean CO_2 Atlas (SOCAT), manuscript in preparation, 2011)). New data of recent cruises in 2010 and 2011 are additionally provided (cf. auxiliary material).

[1]LOCEAN, IPSL, CNRS, Université Pierre et Marie Curie, Paris, France.

0094-8276/11/2011GL049614

[1]Auxiliary materials are available in the HTML. doi:10.1029/2011GL049614.

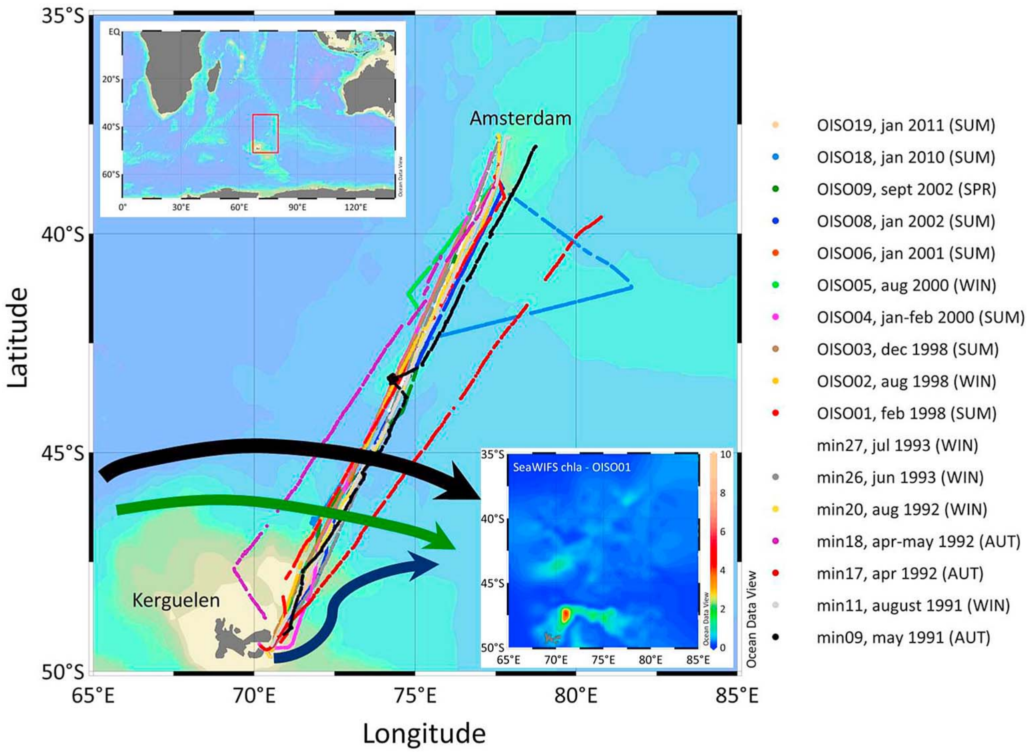

Figure 1. Ship tracks along the Kerguelen- Amsterdam transect of all cruises studied. The legend provides information on month and year of each cruise, while in brackets lie the austral seasons (SPR = spring [sept–nov]; SUM = summer [dec–feb]; AUT = autumn [mar–may]; WIN = winter [jun–aug]). The black arrow corresponds to the Antarctic Circumpolar Current (ACC) core, the green arrow is the northern branch of a current originating in the western Kerguelen plateau and the blue arrow is the eastern extension of the Polar Front [*Park et al.*, 2008]. The upper left framed image captures the extended area of our study. The lower right framed sketch represents the distribution of surface chla (case of OISO01, SeaWIFS, units in mg m^{-3}), where the plume follows the local current configuration.

[6] Average net FCO_2 across the air-sea interface was determined from the formula:

$$FCO_2 = k \times s \times \Delta fCO_2 \quad (1)$$

k is the piston velocity evaluated by *Wanninkhof* [1992]; s the solubility of CO_2 in seawater at the *in situ* temperature and salinity, calculated from *Weiss* [1974] algorithm; ΔfCO_2 is the difference between surface seawater CO_2 (fCO_2^{sw}) and CO_2 in the atmosphere (fCO_2^{air}):

$$\Delta fCO_2 = fCO_2^{sw} - fCO_2^{air} \quad (2)$$

The equation (2) indicates that the ocean acts as a source when $\Delta fCO_2 > 0$ and as a sink when $\Delta fCO_2 < 0$. We used monthly wind speed NCEP/NCAR reanalysis derived data over a grid of 0.5° × 0.5° resolution, provided by NOAA, USA [*Kalnay et al.*, 1996].

3. Results and Discussion

3.1. Co-evolution of Summer fCO_2 With Hydro-bio-geo-physical Signals in the SAZ

[7] Figure 2 illustrates an austral summer bloom case study and the evolution of fCO_2 together with physical, biological and geological parameters along the selected track. The chosen cruise (oiso06, summer 2001) displays an important summer sink (not the most important one, though, cf. section 3.3; Figure 3b), while the additional parameters do not exhibit significant differences compared to other cruises. We first focus on a single cruise as representative because it allows a detailed examination of fCO_2 dynamics along latitudes while interannual trends will be discussed later on (section 3.3).

[8] The most persistent fCO_2 minimum (of >100 μatm, Figure 2c) located at ~47°S (southern hatched area, Figure 2) coincides with a maximum in fluorescence and *in situ* [chla] (Figure 2b), within relatively calm waters (velocity of ~0 cm s^{-1}, Figures 2e and 2f) and occurs just before the most abrupt bathymetric change (Figure 2a). This sharp topographic break is further accompanied by the strongest southward current (up to 1.2 m s^{-1}, Figure 2f). A second smoother fCO_2 trough is manifested at the extreme south of the studied area (~49.5°S) within coastal waters, also associated with a proportional maximum in fluorescence. The SAF (northern hatched area) is associated with a fCO_2 decline of more than 55% compared to the southern one (Figure 2c), but, most importantly, it coincides with an eastward jet of up to 1.6 m s^{-1}, very possibly related to the "ACC Core" [*Park et al.*, 2008] (Figures 1 and 2e). This jet, together with the SAF, clearly separates surface waters along a north-south gradient, while the SSAF waters are constrained among bathymetric (south) and physical (north) limitations. Fe can be therefore diffused by the shallow topography of the NE Kerguelen plateau to surface waters, then be carried away along a NE direction (Figures 1, 2e,

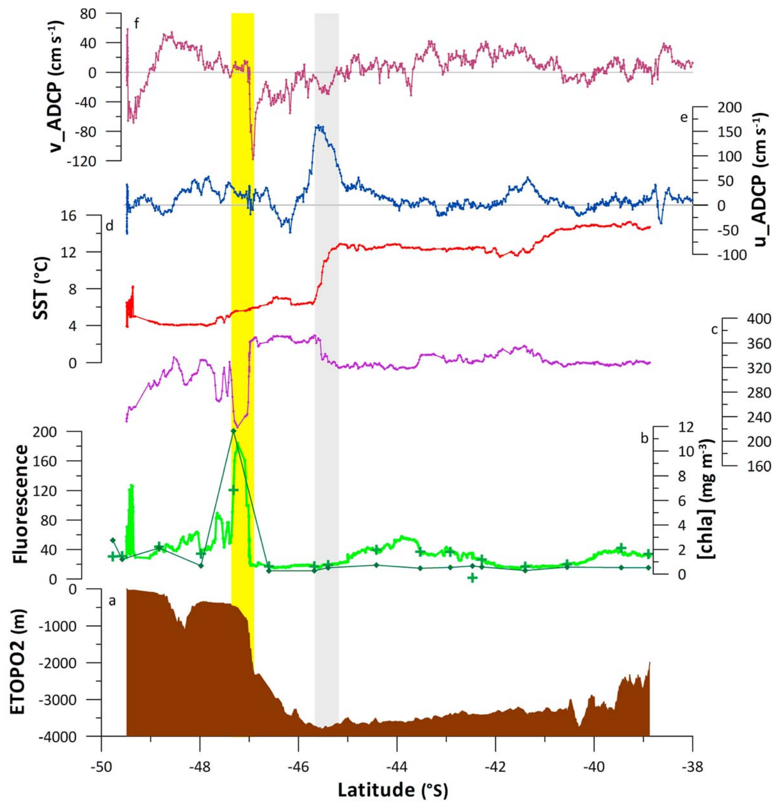

Figure 2. Case-study of a typical austral summer cruise (OISO06) and the evolution with latitude of (a) bathymetry, (b) fluorescence, superimposed with *in situ* [chla], (c) fCO_2, (d) SST (Sea Surface Temperature), (e) the east-west gradient of ADCP (Acoustic Doppler Current Profiler), positive values going eastwards and (f) the north-south gradient of ADCP, positive values going northwards. Grey lines in Figures 2e and 2f are "zero lines". The two hatched areas (going northwards) highlight: (i) the most important fCO_2 drawdown and (ii) the SAF as depicted by abrupt SST changes, the SSS showing a similar pattern (cf. Figure 3b). Dark crosses in fluorescence (Figure 2b) coincident with [chla] sampling timing. ADCP data are from surface (31 m) waters.

and 2f), provoking an intense bloom within a calm area just before the merging of the northern branch of the eastward flow originating from the NW corner of the Kerguelen plateau with the northward Polar Front tongue and their consecutive united Southward transit [*Park et al.*, 2008] (Figures 1 and 2f). Such a mechanism, already evoked through modeling means for the SE Kerguelen plateau bloom [*Maraldi et al.*, 2009], highlight the mesoscale character of the studied area [*Blain et al.*, 2001]. Both the SAF and the intense eastward jet centered at ~45.5°S, prohibit any possibility of Fe transmission further northwards, thus leading to different biogeochemical properties of surface waters. Indeed, within NSAF, [chla] sharply declines by ~90% (Figure 1) and is maintained stable together with fCO_2 (~0.3 mg m^{-3} and 330 μatm, respectively), similar to winter and spring mean values (data not shown). This clearly reveals the dominant biological imprint on fCO_2 distribution within the SSAF during summer season, while the bloom position and intensity are driven by local bathymetric and physical limitations.

3.2. Seasonal fCO_2 Evolution and Annual Mean Fluxes Computing at NSAF and SSAF

[9] We henceforth put into perspective the outcomes of section 3.1 by presenting the ensemble of data from all cruises. Figure 3 sketches the evolution of hydrological parameters (SST and SSS) along with ΔfCO_2 against latitude, grouped by season. Here we focus on meridional variations of SST, SSS and ΔfCO_2 for each season, outside the SAF, without considering temporal changes. The average values of all data treated ($N > 6000$), for both SSAF and NSAF and for every season, are shown in Table 1.

[10] Overall, consistent seasonal hydrological structures are deduced when comparing SSAF with NSAF, the northern being warmer by ~8.5°C and saltier by ~1.2 units than the southern sector, throughout a year. These important hydrological changes across the front are not accompanied by large ΔfCO_2 oscillations (at least not the largest, cf. also Figures 2c and 2d). Moreover, the seasonal meridional ΔfCO_2 shift is not as uniform as displayed by hydrology. The most significant north-south divergence of 33 μatm occurs at spring, to be followed by winter and autumn with >25 μatm, while summer does not encounter major differences (2 μatm). The most striking pattern concerns the sea-air ΔfCO_2 within SSAF, the NSAF area being a relatively constant sink of atmospheric CO_2 of ~30 μatm throughout a year (Figure 3 and Table 1): a large drawdown of up to 185 μatm from spring to summer (Figures 3a and 3b and Table 1) occurs in the SSAF, related to the summer bloom observed in the NE Kerguelen plateau, as seen in our case study (Figure 2c). This large drawdown occurs at the northern limit of the SSAF (situated at ~47°S) and not at

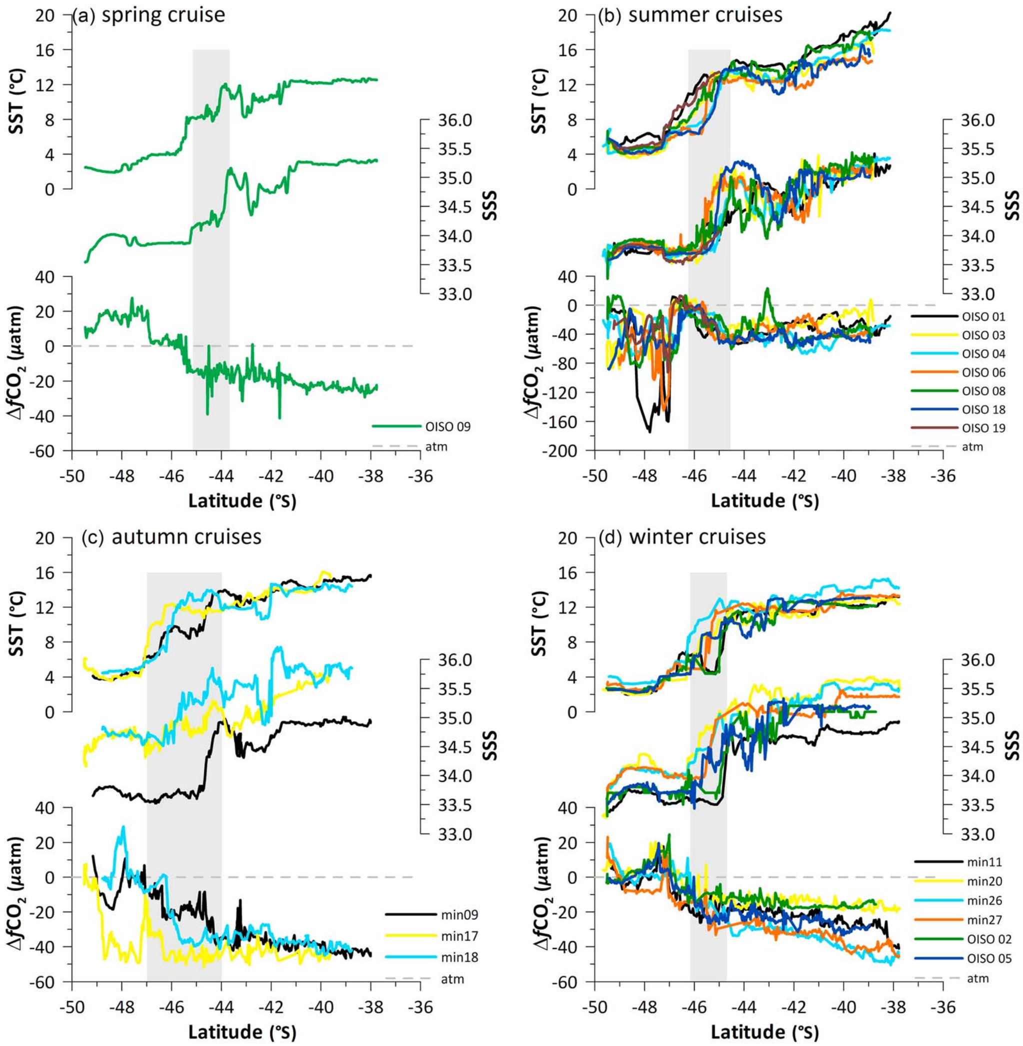

Figure 3. Latitudinal evolution of SST (upper plots), SSS (Sea Surface Salinity, middle plots) and $\Delta f CO_2$ (lower plots) for the ensemble of austral (a) spring, (b) summer, (c) autumn and (d) winter cruises. The shadowed latitude band for all seasons features the hydrological imprint of the SAF, defined by a concomitant abrupt increase of SST and SSS going northwards for every single cruise and corresponds to the northern hatched area in Figure 2. The "zero" dotted line depicts the saturation state for $\Delta f CO_2$. The $\Delta f CO_2$ y-scale for summer period differs from that of other seasons.

the front itself (Figures 2 and 3b), for the ensemble of summer cruises.

[11] Mean seasonal computed FCO_2 for both areas, are shown in Figure 4. While the FCO_2 pattern clearly follows that of $\Delta f CO_2$ ($R > 0.95$, $p < 0.01$) for both long-range winter/summer periods within the SSAF, this is not the case for the NSAF, where the initial more important summer sink (originated from $\Delta f CO_2$) becomes less efficient than the winter one (computed FCO_2), the stronger winter winds by +40% compared to those in summer driving this "sink efficiency" inversion (Figures 4f–4h). Overall, wind speeds were more moderate towards the values previously mentioned for SSAF of 14 m s^{-1} for winter and 7 m s^{-1} for summer [*Pondaven et al.*, 1998]. A second series of wind speeds from CERSAT, IFREMER, provide similar results as NCEP/NCAR (Figure S1). The mean summer SSAF fluxes

Table 1. Average Values for SST, SSS, $\Delta f CO_2$ and FCO_2, South and North of the SAF for Every (Austral) Season[a]

	SST (°C)		SSS		$\Delta f CO_2$ (µatm)		FCO_2 (mmol C m^{-2} d^{-1})	
	SSAF	NSAF	SSAF	NSAF	SSAF	NSAF	SSAF	NSAF
Spring	3.0 (0.8) N = 1; n = 201	11.7 (1.1) N = 1; n = 282	33.9 (0.1)	35.1 (0.2)	+11.8 (7.3)	−21.2 (4.4)	+5.4 (3.4)	−5.8 (1.2)
Summer	5.6 (1.2) N = 7; n = 1144	14.2 (1.8) N = 6; n = 1769	33.7 (0.1)	34.9 (0.3)	−36.4 (30.7)	−38.7 (11.9)	−14.7 (7.4)	−6.6 (1.8)
Autumn	5.6 (2.0) N = 3; n = 320	13.6 (1.2) N = 3; n = 607	34.1 (0.5)	35.1 (0.5)	−14.1 (16.5)	−39.2 (5.7)	−3.3 (3.8)	−10.8 (2.8)
Winter	3.5 (1.2) N = 6; n = 608	12.3 (1.1) N = 6; n = 1168	33.8 (0.2)	35.1 (0.3)	−0.6 (9.1)	−26.1 (9.3)	−0.2 (2.0)	−9.5 (3.3)

[a]Numbers in brackets correspond to the standard deviation among all data of cruises of the same season. *N* indicates the number of cruises and *n* the number of data treated.

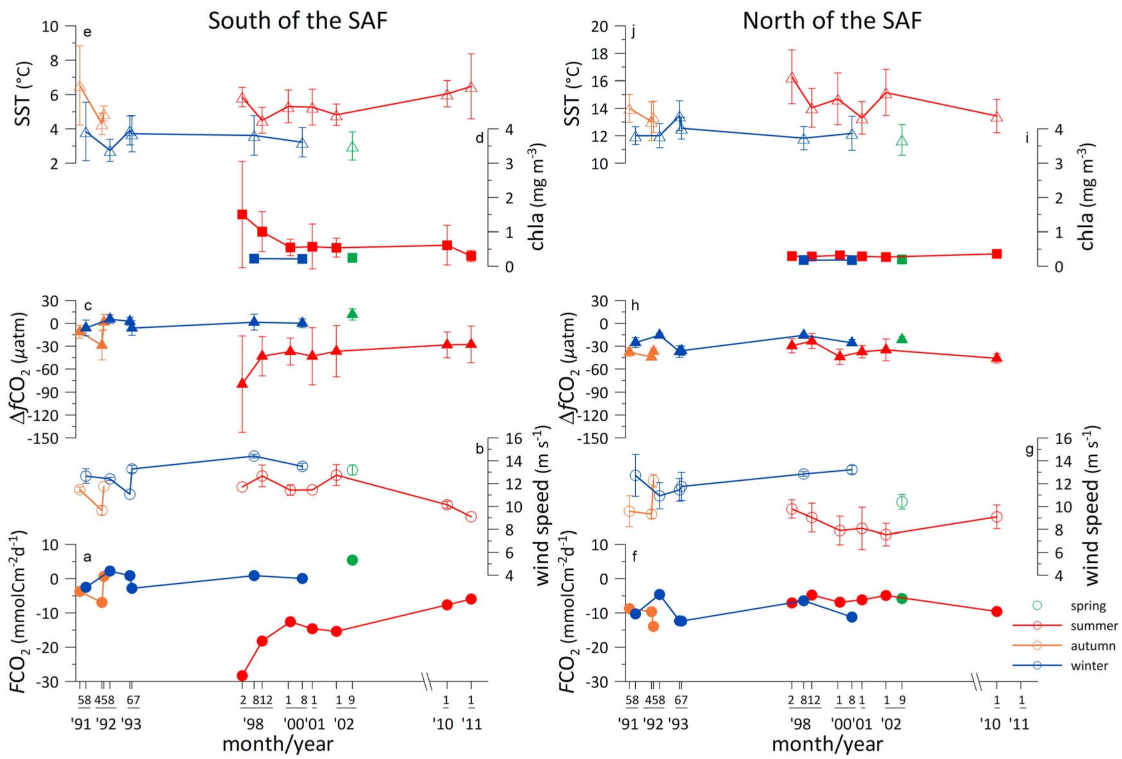

Figure 4. (a, f) Temporal evolution of FCO_2 (filled circles), (b, g) wind speed (open circles), (c, h) $\Delta f CO_2$ (filled triangles), (d, i) satellite-derived [chla] (filled squares) and (e, j) SST (open triangles) for austral spring (green), summer (red), autumn (brown) and winter (blue), in the (left) southern and (right) northern part of the SAF. The y-scales for all variables at SSAF and NSAF are the same, except for SST.

(-14.7 mmol C m^{-2} d^{-1}) are of the same order of magnitude as the 9–24 mmol C m^{-2} d^{-1} summer flux found downstream Crozet island by *Bakker et al.* [2007] -our monthly mean winds were still not corrected for 10 m, which would have resulted in higher values-, as well as with the summer flux of 27.6 mmol C m^{-2} d^{-1} given by *Jouandet et al.* [2008] for the SE Kerguelen plateau -their k formula doubling their values over ours-.

[12] The sum of trimestral extrapolations gives a net sink of -3.0 mol C m^{-2} y^{-1} (-35.9 g C m^{-2} yr^{-1}) for the NSAF, 3-fold more important than that computed for the SSAF (-1.2 mol C m^{-2} yr^{-1} or -13.8 g C m^{-2} yr^{-1}). Moreover, the NSAF sink is found of the same order of magnitude as the updated Takahashi climatology, of -2.4 mol C m^{-2} yr^{-1} (-28.9 g C m^{-2} yr^{-1}), covering two 4° latitude × 5° longitude gridded boxes, centered at -40°S and -44°S, with common 77.5°E longitude (http://www.ldeo.columbia.edu/res/pi/CO2/carbondioxide/pages/air_sea_flux_2010.html). On the contrary, the SSAF sink is 6-fold more important than the mean flux of -0.2 mol C m^{-2} yr^{-1} (-2.3 g C m^{-2} yr^{-1}) estimated by Takahashi climatology, for the closest 48°S/72.5°E-centered gridded box. This points the importance of examination of key sink areas before proceeding to spatial integrations.

3.3. Decadal Summer/Winter Trends and Driving Mecanisms Across the SAF

[13] This section focuses on temporal variabilities of FCO_2 and associated parameters along SSAF and NSAF, illustrated in Figure 4. The discussion is restricted on summer and winter seasons for long-term variations because fall and spring cruises were too limited. Summer (1998–2011) manifests contradictory $\Delta f CO_2$ patterns within SSAF and NSAF: while an increasing trend (+2.3 μatm yr^{-1}, R = 0.68, $p < 0.01$, Figure 4c) is recorded in SSAF, in NSAF the trend is decreasing (-1.4 μatm yr^{-1}, R = -0.69, $p < 0.01$, Figure 4h). This clearly implies that the oceanic $f CO_2$ increases faster than the atmospheric $f CO_2$ at the SSAF (+4.2 μatm yr^{-1}, R = 0.86, $p < 0.01$), contrary to NSAF where the atmospheric $f CO_2$ rises faster than the oceanic $f CO_2$ (no trend retrieved for the latter). This further suggests decreasing and increasing sink patterns for SSAF and NSAF, respectively. Indeed, the area comprising the NE Kerguelen plateau exhibits a decline of carbon sink of 1.2 mmol C m^{-2} d^{-1} yr^{-1} (R = 0.83, $p < 0.01$, Figure 4a), whereas NSAF reveals an increasing carbon sink of 0.3 mmol C m^{-2} d^{-1} yr^{-1} (R = -0.72, $p < 0.01$, Figure 4f), during summer.

[14] Austral winter (1991–2000) is found more homogeneous for the majority of variables, in both SSAF and NSAF. While $f CO_2$ rises by $\sim$2 μatm yr^{-1} (R > 0.65, $p < 0.01$), no particular trend is observed neither for $\Delta f CO_2$ (implying that ocean and atmosphere experience similar $f CO_2$ increase rates, Figures 4c and 4h) nor for FCO_2 (Figures 4a and 4f), despite the fact that wind speeds show an increasing pattern on both sides of the front (+0.2 m s^{-1} yr^{-1}, R $\sim$ 0.65, $p <$ 0.01, Figures 4b and 4g). On the contrary, in SSAF an important decline of wind speed takes place exclusively during summer (-0.2 m s^{-1} yr^{-1}, R = -0.85, $p < 0.01$, Figure 4b). Overall, in the sector where winds decrease, the CO_2 sink declines (SSAF in summer, Figures 4b and 4a), whereas when they get stronger, no clear FCO_2 pattern is observed (winter, Figures 4b, 4g, 4a, and 4f). More extended

model-inversion outcomes associate a westerlies strengthening with a decline in CO_2 sink, south of the Polar Front [*Le Quéré et al.*, 2007; *Lenton et al.*, 2009]. Our study provides an insight into the processes of the CO_2 sink fate further northwards over a time and space-restricted frame.

[15] Neither temporal temperature change, nor sampling biases can be responsible for the doubled summer fCO_2 increase compared to winter, within the SSAF. A probable reason lies in the initial summer year 1998, an important ENSO (El Niño Southern Oscillation) year, associated with an elevated SAM index (Southern Annular Mode) [*Marshall*, 2003], accompanied by an elevated SST signal in the Western Indian basin [*Murtugudde et al.*, 2000]. We suspect that this warming also propagated southwards [*Jabaud-Jan et al.*, 2004], also seen in our data (Figure 4e), provoking advanced water productivity (as demonstrated by [chla], Figure 4d) that led to an exceptional fCO_2 decrease (Figure 4c) in summer 1998. The ENSO impact is further depicted in the NSAF, with increased SST, reduced fCO_2, elevated [chla] and increased CO_2 sink (Figures 4j, 4h, 4i, and 4f) but of much lesser extent than that observed for the SSAF, due to limited proximity to the fertile plateau (Figure 2a).

[16] No correlation is deduced between SST and fCO_2 during summer in SSAF. This contrasts with the SE Kerguelen plateau where the modeling outcome of *Jouandet et al.* [2011] suggests dominant solubility effects. On the opposite, we find a significant anti-correlation between ΔfCO_2 and [chla] ($R = -0.92$, $p < 0.01$), implying a dominant biological imprint in the SSAF during summer. Still, [chla] decreases with time (Figure 4d). We therefore speculate that the weaker summer sink within the SSAF is driven by weaker water mixing as supported by the declining winds, yielding to warmer waters (increasing SST pattern). Less mixing would also imply reduced Fe alimentation and thus less productivity (declined [chla]), leading to less CO_2 uptake (increasing fCO_2). The decline in CO_2 sink caused by reduced summer winds within SSAF is supported by two different satellite-derived datasets (Figure S1). These wind trends, together with [chla] weakening pattern and SST anomaly, are further put into perspective with long-term summer decreasing climatological indexes (Multivariate ENSO Index -MEI-, SAM) in Figure S2. The summer fCO_2 increase in the last two years can be additionally caused by oceanic warming induced by the atmosphere (Figure 4e), which adds to the warming due to water mixing decline suggestion.

[17] An anti-correlation between ΔfCO_2 and [chla] ($R = -0.70$, $p < 0.01$) is also seen for the NSAF, suggesting biological summer influences for both sides of the front, but of opposite patterns. Winter SSAF shows a weak anti-correlation between fCO_2 and SST, which becomes more important at NSAF ($R = -0.50$ to -0.79, $p < 0.01$). This translates to vertical mixing processes dominance during winter. Overall, the opposing sides of the front are subject to similar main seasonal processes (vertical mixing in winter, biology in summer) as already shown by *Metzl et al.* [1999] for the entire SAZ, but display different interannual trends of FCO_2 and associate parameters, unveiling the importance of north/south frontal partitioning initiated in this study.

4. Conclusions

[18] This study provides for the first time 20-yr estimates on fCO_2 dynamics upon two areas separated by the SAF, downstream of Kerguelen islands. An important summer bloom is located at the SSAF, of $-14.7(\pm 7.4)$ mmol C m^{-2} d^{-1}. These fertile and relatively calm waters are constrained by two physical barriers: the shallow topography of Kerguelen plateau at the south, and an eastward jet of up to 1.6 m s^{-1}, at the north. This jet blocks any communication with further north, the NSAF waters displaying lesser but homogeneous seasonal fluxes of ~ -8.5 mmol C m^{-2} d^{-1}. Our data reveal a weakening trend of the SSAF carbon sink with time, probably due to less Fe input, related to weaker water mixing. This sink declines 4 times faster than the NSAF sink increase, which calls for more data acquisition over this area, as well as across other frontal regions, in order to better constrain the island mass effect. The comparison of our results with Takahashi climatology emphasizes the importance of separately examining the carbon budgets at oceanic areas across frontal positions, providing additional spatio-temporal constraints which can be useful for atmospheric inversions and call for better resolution biogeochemical models.

[19] **Acknowledgments.** The OISO program is supported by three French institutes: INSU (Institut National des Sciences de l'Univers), IPSL (Institut Pierre Simon Laplace) and IPEV (Institut Paul Emile Victor). This study was also supported by the national French program LEFE/Cyber (project FlamenCO2). We are thankful to the captains and crews of R.S.S. Marion Dufresne and colleagues at LOCEAN for their active participation during the OISO cruises. Many thanks to Annie Kartavtseff for processing the ACDP data and all SOCAT players. M. Ramonet is particularly acknowledged, for providing atmospheric CO_2 data for the austral summer 2010–2011 periods. We further acknowledge the following data platforms: (1) NCEP/NCAR Reanalysis I data provided by the NOAA/OAR/ESRL PSD, Boulder, Colorado, USA, http://www.esrl.noaa.gov/psd/; (2) the Giovanni online data system, developed and maintained by the NASA GES DISC: http://disc.sci.gsfc.nasa.gov/giovanni/; (3) secondary wind speed datasets from CERSAT, IFREMER, Plouzané (France): http://www.ifremer.fr/cersat/en/data/gridded.htm; (4) World Data Centre for Greenhouse Gases (WDCGG) for 2010 atmCO_2 data: http://gaw.kishou.go.jp/wdcgg/; (5) Schlitzer R., for the Ocean Data View software, http://odv.awi.de. The authors finally thank D. Cardinal, Dr Rhou, VVSS Sarma and an anonymous reviewer for their constructive comments on previous versions of this work.

[20] The Editor thanks V.V.S.S. Surma and an anonymous reviewer for their assistance in evaluating this paper.

References

Bakker, D. C. E., M. C. Nielsdóttir, P. J. Morris, H. J. Venables, and A. J. Watson (2007), The island mass effect and biological carbon uptake for the subantarctic Crozet Archipelago, *Deep Sea Res., Part II*, *54*(18–20), 2174–2190, doi:10.1016/j.dsr2.2007.06.009.

Blain, S., et al. (2001), A biogeochemical study of the island mass effect in the context of the iron hypothesis: Kerguelen Islands, Southern Ocean, *Deep Sea Res., Part I*, *48*(1), 163–187, doi:10.1016/S0967-0637(00)00047-9.

Blain, S., et al. (2007), Effect of natural iron fertilization on carbon sequestration in the Southern Ocean, *Nature*, *446*, 1070–1074, doi:10.1038/nature05700.

Blain, S., G. Sarthou, and P. Laan (2008), Distribution of dissolved iron during the natural iron-fertilization experiment KEOPS (Kerguelen Plateau, Southern Ocean), *Deep Sea Res., Part II*, *55*(5–7), 594–605, doi:10.1016/j.dsr2.2007.12.028.

Chever, F., G. Sarthou, E. Bucciarelli, S. Blain, and A. R. Bowie (2010), An iron budget during the natural iron fertilisation experiment KEOPS (Kerguelen Islands, Southern Ocean), *Biogeosciences*, *7*, 455–468, doi:10.5194/bg-7-455-2010.

Doty, M. S., and M. Oguri (1956), The island mass effect, *J. Cons. Int. Explor. Mer.*, *22*, 33–37.

Jabaud-Jan, A., N. Metzl, C. Brunet, A. Poisson, and B. Schauer (2004), Interannual variability of the carbon dioxide system in the southern Indian Ocean (20°S–60°S): The impact of a warm anomaly in austral summer 1998, *Global Biogeochem. Cycles*, *18*, GB1042, doi:10.1029/2002GB002017.

Jouandet, M.-P., S. Blain, N. Metzl, C. Brunet, T. W. Trull, and I. Obernosterer (2008), A seasonal carbon budget for a naturally iron-fertilized bloom over the Kerguelen Plateau in the Southern Ocean, *Deep Sea Res., Part II*, *55*(5–7), 856–867, doi:10.1016/j.dsr2.2007.12.037.

Jouandet, M.-P., S. Blain, N. Metzl, and M. Mongin (2011), Interannual variability of net community production and air-sea CO_2 flux in a naturally iron fertilized region of the Southern Ocean (Kerguelen plateau), *Antarct. Sci.*, *23*(6), 589–596, doi:10.1017/S0954102011000411.

Kalnay, E., et al. (1996), The NCEP/NCAR 40-year reanalysis project, *Bull. Am. Meteorol. Soc.*, *77*(3), 437–471, doi:10.1175/1520-0477(1996)077<0437:TNYRP>2.0.CO;2.

Lenton, A., F. Codron, L. Bopp, N. Metzl, P. Cadule, A. Tagliabue, and J. Le Sommer (2009), Stratospheric ozone depletion reduces ocean carbon uptake and enhances ocean acidification, *Geophys. Res. Lett.*, *36*, L12606, doi:10.1029/2009GL038227.

Le Quéré, C., et al. (2007), Saturation of the Southern Ocean CO_2 sink due to recent climate change, *Science*, *316*(5832), 1735–1738, doi:10.1126/science.1136188.

Lourantou, A., J. V. Lavrič, P. Köhler, J.-M. Barnola, E. Michel, D. Paillard, D. Raynaud, and J. Chappellaz (2010a), A detailed carbon isotopic constraint on the causes of the deglacial CO_2 increase, *Global Biogeochem. Cycles*, *24*, GB2015, doi:10.1029/2009GB003545.

Lourantou, A., J. Chappellaz, J.-M. Barnola, V. Masson-Delmotte, and D. Raynaud (2010b), Changes in atmospheric CO_2 and its carbon isotopic ratio during the penultimate deglaciation, *Quat. Sci. Rev.*, *29*(17–18), 1983–1992, doi:10.1016/j.quascirev.2010.05.002.

Maraldi, C., M. Mongin, R. Coleman, and L. Testut (2009), The influence of lateral mixing on a phytoplankton bloom: Distribution in the Kerguelen Plateau region, *Deep Sea Res., Part I*, *56*(6), 963–973, doi:10.1016/j.dsr.2008.12.018.

Marshall, G. J. (2003), Trends in the Southern Annular Mode from observations and reanalyses, *J. Clim.*, *16*, 4134–4143, doi:10.1175/1520-0442(2003)016<4134:TITSAM>2.0.CO;2.

Martin, J. H. (1991), Iron still comes from above, *Nature*, *353*, 123, doi:10.1038/353123b0.

Metzl, N. (2009), Decadal increase of oceanic carbon dioxide in Southern Indian Ocean surface waters (1991–2007), *Deep Sea Res., Part II*, *56*(8–10), 607–619, doi:10.1016/j.dsr2.2008.12.007.

Metzl, N., B. Tilbrook, and A. Poisson (1999), The annual fCO_2 cycle and the air–sea CO_2 flux in the sub-Antarctic Ocean, *Tellus, Ser. B*, *51*(4), 849–861, doi:10.1034/j.1600-0889.1999.t01-3-00008.x.

Mikaloff Fletcher, S. E., et al. (2006), Inverse estimates of anthropogenic CO_2 uptake, transport, and storage by the ocean, *Global Biogeochem. Cycles*, *20*, GB2002, doi:10.1029/2005GB002530.

Mongin, M., E. Molina, and T. W. Trull (2008), Seasonality and scale of the Kerguelen plateau phytoplankton bloom: A remote sensing and modeling analysis of the influence of natural iron fertilization in the Southern Ocean, *Deep Sea Res., Part II*, *55*(5–7), 880–892, doi:10.1016/j.dsr2.2007.12.039.

Murtugudde, R., J. P. McCreary, and A. J. Busalacchi (2000), Oceanic processes associated with anomalous events in the Indian Ocean with relevance to 1997–1998, *J. Geophys. Res.*, *105*(C2), 3295–3306, doi:10.1029/1999JC900294.

Park, Y.-H., L. Gamberoni, and E. Charriaud (1993), Frontal structure, water masses, and circulation in the Crozet Basin, *J. Geophys. Res.*, *98*(C7), 12,361–12,385, doi:10.1029/93JC00938.

Park, Y.-H., N. Gasco, and G. Duhamel (2008), Slope currents around the Kerguelen Islands from demersal longline fishing records, *Geophys. Res. Lett.*, *35*, L09604, doi:10.1029/2008GL033660.

Planquette, H., et al. (2007), Dissolved iron in the vicinity of the Crozet Islands, Southern Ocean, *Deep Sea Res., Part II*, *54*(18–20), 1999–2019, doi:10.1016/j.dsr2.2007.06.019.

Pondaven, P., C. Fravalo, D. Ruiz-Pino, P. Treguer, B. Queguiner, and C. Jeandel (1998), Modelling the silica pump in the permanently open ocean zone of the Southern Ocean, *J. Mar. Syst.*, *17*, 587–619, doi:10.1016/S0924-7963(98)00066-9.

Sabine, C. L., et al. (2004), The oceanic sink for anthropogenic CO_2, *Science*, *305*(5682), 367–371, doi:10.1126/science.1097403.

Takahashi, T., et al. (2009), Climatological mean and decadal change in surface ocean pCO_2, and net sea-air CO_2 flux over the global oceans, *Deep Sea Res., Part II*, *56*(8–10), 554–577, doi:10.1016/j.dsr2.2008.12.009.

Wanninkhof, R. (1992), Relationship between wind speed and gas exchange over the ocean, *J. Geophys. Res.*, *97*(C5), 7373–7382, doi:10.1029/92JC00188.

Weiss, R. F. (1974), Carbon dioxide in water and seawater: The solubility of a non-ideal gas, *Mar. Chem.*, *2*, 203–215, doi:10.1016/0304-4203(74)90015-2.

A. Lourantou and N. Metzl, LOCEAN, IPSL, CNRS, Université Pierre et Marie Curie, Case 100, 4 place Jussieu, F-75252 Paris CEDEX 05, France. (anna.lourantou@locean-ipsl.upmc.fr)